First-principles investigation of phase stability in the Mg-Sc binary alloy

Anirudh Raju Natarajan and Anton Van der Ven

First principles investigation of phase stability in the Mg-Sc binary alloy

Anirudh Raju Natarajan[1] and Anton Van der Ven[1, *]

[1]*Materials Department, University of California, Santa Barbara*

(Dated: April 25, 2017)

The recent discovery of shape memory behavior in Mg-Sc alloys has opened the door to the possibility of lightweight shape memory alloys. Very little is known, however, about martensitic phase transformations or about equilibrium phase stability in this alloy system. Here we report on a first-principles statistical mechanics study of zero Kelvin and finite temperature phase stability of HCP, BCC and FCC based phases in the Mg-Sc binary. Our calculations reveal a rich array of phase transitions among the different low-temperature ordered and high-temperature disordered phases. Ground state orderings on HCP, BCC and FCC belong to families of hierarchical structures containing rods of scandium atoms assembled in layers that repeat periodically. Both FCC and BCC are found to undergo a series of second-order phase transformations with increasing temperature until they completely disorder. A high degree of degeneracy is predicted at low and high temperatures among HCP, BCC and FCC, a property that is likely to play an important role in the shape memory effects observed in this alloy.

I. INTRODUCTION

Growing demand for light weight materials in industrial applications, ranging from cellular phones to automobiles, has led to vigorous research into magnesium based alloys[1,2]. While Mg alloys are actively being developed to replace heavier materials in structural applications, a recent study by Ogawa *et al.*[3] on Mg-Sc alloys has opened the possibility that these lightweight alloys may also be viable for shape memory applications.

The study by Ogawa *et al.*[3] was inspired by the similarities between the Mg-Sc binary phase diagram and those of titanium alloys that show the shape-memory effect. By quenching a BCC Mg-Sc alloy down to 123K, Ogawa *et al.*[3] were able to demonstrate the onset of superelasticity upon straining. The study showed the formation of temperature induced martensite at low scandium compositions, but only stress induced martensites at higher scandium contents[3]. Although the formation of an HCP based martensite was reported, the identity of the superelastic phase remains unclear.

Unlike some of the other rare-earth based magnesium alloys[2,4–7], very little is known about phase stability in the Mg-Sc binary system. The first extensive study of the magnesium-rich portion of this phase diagram was performed by Beaudry and Dane[8]. They used a combination of thermal, metallographic and X-Ray methods to study alloys having scandium compositions up to 60 at.% and established the liquidus and solidus curves in the magnesium rich part of the phase diagram. The study also reported the formation of a disordered B2 (CsCl type) phase at scandium compositions around 30%. Alloys with similar compositions at higher temperatures were observed to form a disordered BCC solid solution. Higher scandium contents (50%) that were annealed at 450°C did not show the formation of any phases other than an additional disordered scandium-rich HCP phase. Subsequent studies[9,10] were in qualitative agreement with the observations by Beaudry[8]. More recent work by Ogawa *et al.*[11,12] using diffusion couples helped establish the

bounds of a two-phase region separating a Mg-rich HCP solid solution (α) and a BCC solid solution (β).

The limited experimental data about phase stability in the Mg-Sc binary motivates a number of questions. All experimental studies to date have primarily focused on the high temperature behavior of this alloy system. Very little is known about the low-temperature region of the phase diagram or about the existence of metastable phases that may play a role in the observed shape memory effect. A previous first-principles investigation of the formation energies of several crystal structures and orderings in the Mg-Sc binary predicted the stability of an FCC based ordering at intermediate scandium compositions as well as an HCP-based ordering at higher scandium compositions[13]. Neither of these orderings have been observed at high temperature. A peculiar feature of the currently assessed Mg-Sc binary phase diagram is the remarkably wide composition interval in which a B2 phase is reported to be stable. While a perfectly ordered B2 phase (CsCl ordering on a BCC lattice) has a composition of $x_{Sc} = 0.5$, experimental evidence in the Mg-Sc binary suggests a B2 phase that can tolerate a 20% excess of Mg[8]. The mechanism with which the excess Mg is accommodated and the degree of disorder it introduces in the B2 phase is not known. Yet the off-stoichiometry and order-disorder phenomena in Mg rich BCC likely play an important role in the shape memory effect observed in these alloys.

Ab-initio approaches have proven valuable in shedding light on shape memory phenomena in titanium[14–16] and nickel[17–22] based alloys. Here we study finite temperature phase stability in the Mg-Sc binary alloy from first-principles. Formation energies calculated from first-principles of symmetrically distinct orderings on the HCP, BCC and FCC crystal structures show the stability of hierarchical orderings on the global and metastable convex hulls. HCP and FCC based orderings are found to be energetically competitive at scandium compositions ranging from $x_{Sc} = 0.125$ to $x_{Sc} = 0.5$, with BCC based orderings having comparable energies in a rela-

tively small composition window centered around $x_{Sc} = 0.35$. The low energy FCC based orderings are surprising since there is no experimental evidence for FCC at high-temperature. Free energies calculated with Monte Carlo simulations applied to cluster expansions parameterized from first-principles show that all three crystal structures are predicted to form disordered solid solutions at relatively low temperatures. A wide stability range is predicted for B2 ordering on BCC, with off-stoichiometry accommodated by excess Mg on the Sc sublattice. The calculated metastable BCC phase diagram at Mg rich compositions where shape memory effects are observed experimentally shows a second order phase transition separating Mg-excess B2 at high temperature from a low temperature ordering at a composition of $x_{Sc} = 0.25$. We find that global phase stability among HCP, BCC and FCC at intermediate and high temperatures is very sensitive to small perturbations to their free energies. This indicates a high degree of degeneracy among HCP, FCC and BCC in Mg-Sc, which is likely to have important consequences for observed martensitic transformations.

II. METHODS

Total energies at 0K for orderings on a crystal structure were calculated within the Perdew-Burke-Ernzerhof (PBE) parameterization of the generalized gradient approximation (GGA)[23] to density functional theory (DFT). Projecter augmented wave (PAW) pseudopotentials with 8 valence electrons for magnesium and 11 valence electrons for scandium were used. Total energies were calculated by relaxing all configurations with respect to their cell shape, size and internal positions of the atoms with the *Vienna Ab-Initio Simulation Package* (VASP)[24–27]. An energy cutoff of 450 eV was used for the plane-wave basis set. A reference $25 \times 25 \times 13$ Γ-centered k-point mesh was used for the HCP magnesium configuration with lattice constants $a = 3.19$Å and $c = 5.18$Å. The grids were scaled appropriately for the larger supercells to contain 67-69 k-points per Å^{-1}.

An arrangement of Mg and Sc atoms over N sites on a crystal can be represented by a vector of occupation variables $\vec{\sigma} = \{\sigma_1, \sigma_2, \cdots, \sigma_N\}$. The occupation variable, σ_i is assigned a value of 0 if magnesium is present at site i or 1 if scandium occupies the site. Formation energies of a configuration ($\vec{\sigma}$) must be defined relative to some reference configurations. In this study we use the total energies of magnesium and scandium in the HCP state at 0K as reference:

$$E_f(\vec{\sigma}) = \frac{E(\vec{\sigma}) - N_{Mg}E_{Mg}^{HCP} - N_{Sc}E_{Sc}^{HCP}}{N_{Mg} + N_{Sc}} \qquad (1)$$

where $E_f(\vec{\sigma})$ is the formation energy of a particular arrangement of atoms ($\vec{\sigma}$) on a crystal, N_{Mg} and N_{Sc} are the number of magnesium and scandium atoms in the

configuration, $E(\vec{\sigma})$ is the total energy for the configuration and E_{Mg}^{HCP} and E_{Sc}^{HCP} are the total energies per atom for magnesium and scandium in the HCP crystal structure at 0K.

Finite temperature free energies and phase stability were calculated by using statistical mechanics approaches as applied to a configurational cluster expansion. A configurational cluster expansion, informed by DFT formation energies, can be used to predict the formation energy of any ordering of atoms on a particular crystal structure. Within this formalism, the formation energy of an ordering of atoms ($\vec{\sigma}$) on a crystal, is parameterized with an expansion of polynomials of site occupation variables according to[28–30]:

$$E_f(\vec{\sigma}) = V_0 + \sum_\alpha V_\alpha \phi_\alpha(\vec{\sigma}) \qquad (2)$$

where the sum extends over all clusters of sites α, the $\phi_\alpha(\vec{\sigma})$ are products of the occupation variables of the sites belonging to the cluster α and V_α are expansion coefficients referred to as effective cluster interactions.

The CASM software package[31–34] was used to enumerate symmetrically distinct orderings on the HCP, FCC and BCC parent crystal structures, parameterize the expansion coefficients of cluster expansions and perform Monte Carlo simulations. Separate cluster expansions for each crystal structure were parameterized using least squares regression on a set of clusters chosen using a genetic algorithm[35]. A k-fold cross-validation score with 15 folds was used to select clusters within the genetic algorithm. In order to increase the accuracy of the cluster expansions for low-energy orderings, all formation energies were weighted with Boltzmann weights dependent on the distance from the metastable convex hull, with a kT around 0.01 eV/atom.

Phase stability at finite temperature was determined by applying the common tangent construction to the free energies of all the relevant phases. Ensemble averages from grand-canonical Monte Carlo (GCMC) applied to the cluster expansions parameterized from first-principles were used in free energy integration schemes to calculate high temperature free energies. Subsequently, phase diagrams were constructed based on the convex hull applied to the calculated free energies. Details of the cluster expansion fits and Monte Carlo calculations are summarized in table I. The cluster expansion for the HCP crystal structure was trained to reproduce the important ground states across the full composition region, while the BCC and FCC cluster expansions were only required to reproduce the grounds states up to a composition of $x_{Sc} = 0.5$.

III. LOW TEMPERATURE PHASE STABILITY

Phase stability at 0K can be predicted by applying the common tangent construction to the formation energies of all relevant orderings. Often, it is useful to consider not just global phase stability but also metastability. For

Type	# train	RMS	wRMS	CV	# Clusters	GCMC size
HCP	505	0.007	0.003	0.003	25	$18 \times 18 \times 8$
FCC	452	0.006	0.003	0.003	23	$12 \times 12 \times 12$
BCC	373	0.010	0.002	0.002	17	$16 \times 16 \times 16$

TABLE I. Details of the cluster expansion and grand canonical Monte Carlo calculations for HCP, BCC and FCC crystal structures. The table lists the root mean square error (RMS), weighted root mean square error (wRMS), cross-validation score (CV), number of clusters, and the size of the GCMC simulation cell. The errors are listed in units of eV/atom.
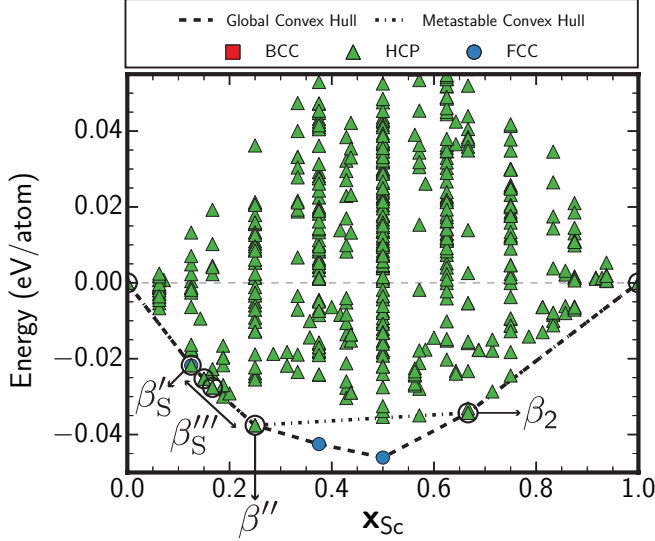

FIG. 1. Formation energies of orderings on the HCP crystal structure calculated with DFT. Both the metastable and global convex hull are shown. Orderings on the metastable convex hull are circled.

FIG. 2. Formation energies of orderings on the BCC crystal structure calculated with DFT. Both the metastable and global convex hull are shown. Orderings on the metastable convex hull are circled. The formation energy of Sc in the BCC crystal structure is 0.103 eV/atom relative to HCP Sc.
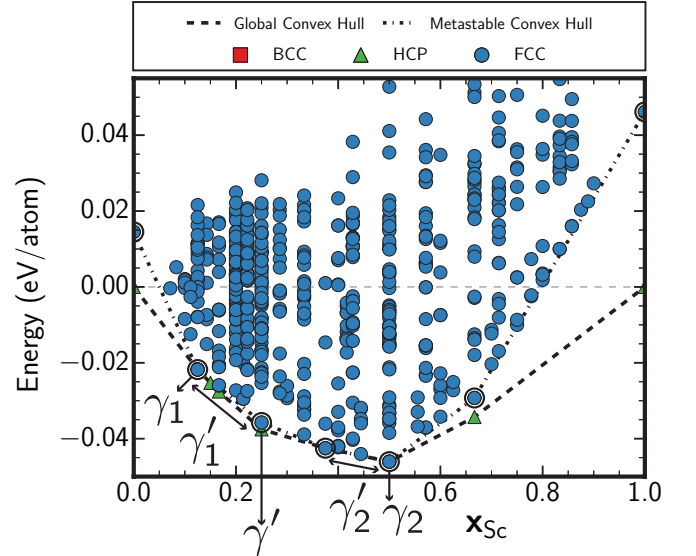
FIG. 3. Formation energies of orderings on the FCC crystal structure calculated with DFT. Both the metastable and global convex hull are shown. Orderings on the metastable convex hull are circled.

instance, during aging heat treatments, metastable precipitates are often formed due to the lower barrier to nucleate them as compared to other phases that might be thermodynamically more stable. Metastable phases may also be formed through a variety of different processing conditions, such as quenching, that freeze in high temperature phases. We start by investigating the orderings that are on the convex hull of the three parent crystal structures that occur in most binary alloys: BCC, HCP and FCC.

A. Formation energies across the individual crystal structures

Formation energies, calculated with DFT, of orderings on the HCP, BCC and FCC crystal structures are shown in figs. 1 to 3. Each figure also shows the global convex hull (evaluated over orderings on all three crystal structures) in addition to the metastable convex hull (indicated by empty black circles).

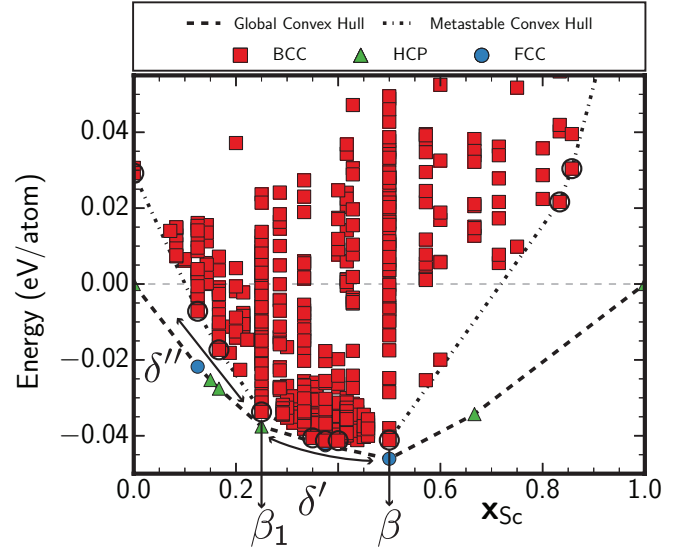Low energy orderings (fig. 1) on HCP are predicted to contain Sc atoms arranged as rods along the [0001] direction. A hierarchy of orderings, that we have labeled β_S''', are predicted to be stable at low scandium compositions between $x_{Sc} = 0.125$ to $x_{Sc} = 0.25$. This family of orderings can be generated by combining the β_S' ordering (fig. 4a), containing Sc rods arranged as "zig-zags" and having a Sc composition $x_{Sc} = 0.125$, with the β'' ordering (fig. 4d), containing Sc rods arranged as hexagons and having a Sc composition $x_{Sc} = 0.25$. The β_S''' family of orderings have compositions that lie between those of the

(a) β'_S
($x_{Sc} = 0.125$)

(b) β'''_S
($x_{Sc} = 0.15$)

(c) β'''_S
($x_{Sc} = 0.1667$)

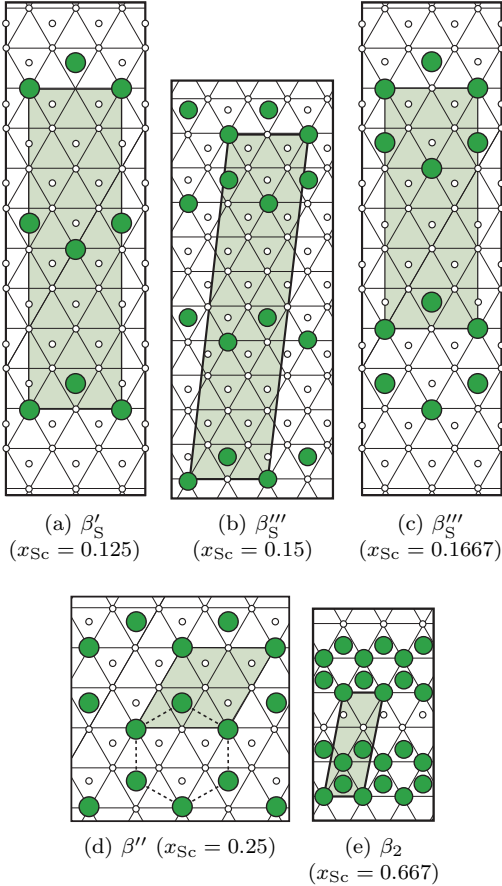(d) β'' ($x_{Sc} = 0.25$)

(e) β_2
($x_{Sc} = 0.667$)

FIG. 4. Schematic crystal structures of orderings on the metastable HCP convex hull. Scandium atoms are drawn in green and magnesium atoms are depicted by the smaller white circles. Orderings are shown as viewed along the [0001] axis. The triangular basal layers are stacked with an "AB"-type stacking when viewed along this axis. The basal plane is denoted by the atoms on the corners of the triangular grid, while the layer above is shown as the atoms that are at the center of the triangles.

parents, β'_S and β''. Figures 4b and 4c show two examples of β'''_S orderings. An in depth discussion of their crystallography as well as a generating algorithm and naming scheme may be found in a previous study[5]. The HCP based ground state ordering at the higher Sc concentration of $x_{Sc} = 0.667$ also consists of Sc rods that arrange as strips of hexagons as shown in fig. 4e. The rods of each hexagon, however, are closer together compared to those in β'' (fig. 4d) and the distance between adjacent strips of hexagons is also closer than in β'''_S (fig. 4c).

Energies and crystal structures of metastable orderings on the BCC crystal structure are shown in figs. 2 and 5. The metastable orderings on BCC consist of chains of scandium atoms along the [001] direction. The simplest of these orderings have compositions of $x_{Sc} = 0.25$ and $x_{Sc} = 0.5$. The phase at $x_{Sc} = 0.5$, shown in fig. 5g and labeled β, is identical to the well-known B2 structure

(CsCl). It may be viewed as a square arrangement of [001] scandium rods. The stable ordering with a composition of $x_{Sc} = 0.25$ is shown in fig. 5c. This ordering consists of chains of alternating Sc and Mg atoms along the [001] direction. Neighboring chains are "out-of-phase", in the sense that they are shifted relative to each other by a single BCC lattice translation. This ordering, referred to in the literature[2] as β_1, is often observed as an equilibrium phase in other Mg-RE alloys.

As with HCP, families of hierarchical orderings are also stable on BCC. Starting from the two simplest metastable orderings, β and β_1, and Mg in the BCC crystal structure, two sets of hierarchical structures may be generated. The first consists of (010) layers consisting of [001] Mg-Sc chains separated by blocks of Mg, as shown in figs. 5a and 5b. The chains of Mg-Sc atoms are similar to those found in the β_1 ordering (fig. 5c). We will label this hierarchy as δ''. At higher scandium concentrations, a second family of orderings emerges by combining layers of β_1 with β along the [010] direction. These δ' orderings consist of layers of scandium rods and Mg-Sc chains arranged within (010) planes. The layers that are fully filled are similar to β while the slabs containing Mg-Sc chains have β_1 ordering. The DFT results suggest that the β_1 and β orderings may be combined along both the [010] and [110] directions. This ordering has a composition of $x_{Sc} = 0.375$, and is energetically degenerate to within the DFT accuracy with the δ' orderings.

While the experimental Mg-Sc phase diagram shows the formation of BCC and HCP based phases, our first-principles calculations and those of Taylor et al.[13] suggest that FCC based orderings are also energetically competitive as illustrated in fig. 3. Similar to the HCP orderings, all metastable FCC orderings consist of rods of Sc atoms arranged along the [001] direction as shown in fig. 6. The stable ordering at a composition of $x_{Sc} = 0.25$ (γ') corresponds to the well known L1$_2$ crystal structure. As shown in fig. 6c, this ordering can be viewed as scandium rods arranged at the corners of the centered-square lattice of the (001) FCC planes. At equiatomic composition ($x_{Sc} = 0.5$), the stable γ_2 ordering consists of two layers of scandium alternating with two layers of magnesium (fig. 6e) along the [010] direction. Lower scandium compositions around $x_{Sc} = 0.125$ promote the formation of an ordering (γ_1) with layers of Sc rods as seen in fig. 6a. This phase may be viewed as layers of Sc rods that are stacked along the [010] direction and separated by three layers of magnesium. Adjacent layers are shifted relative to each other along the [100] direction. A possible hierarchy of structures (γ'_1), ranging in composition from $x_{Sc} = 0.125$ to 0.25, may be generated by combining γ' with γ_1 along the [010] direction as shown in fig. 6b. A particular ordering within this hierarchy is predicted to be less than 1 meV/atom of the metastable convex hull (which is within the DFT error). Our calculations show a second hierarchy of orderings (γ'_2) to also be stable on the FCC crystal structure. The orderings, shown in fig. 6d may be formed by removing a single column of scandium

(a) δ''
$(x_{Sc} = 0.125)$

(b) δ''
$(x_{Sc} = 0.1667)$

(c) β_1 $(x_{Sc} = 0.25)$

(d) δ' $(x_{Sc} = 0.35)$

(e) δ'
$(x_{Sc} = 0.375)$

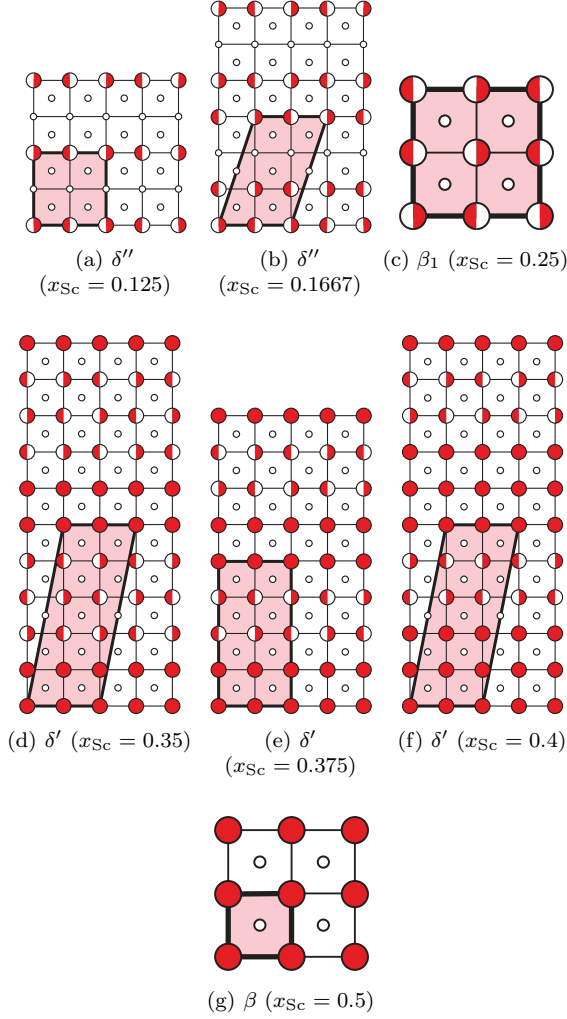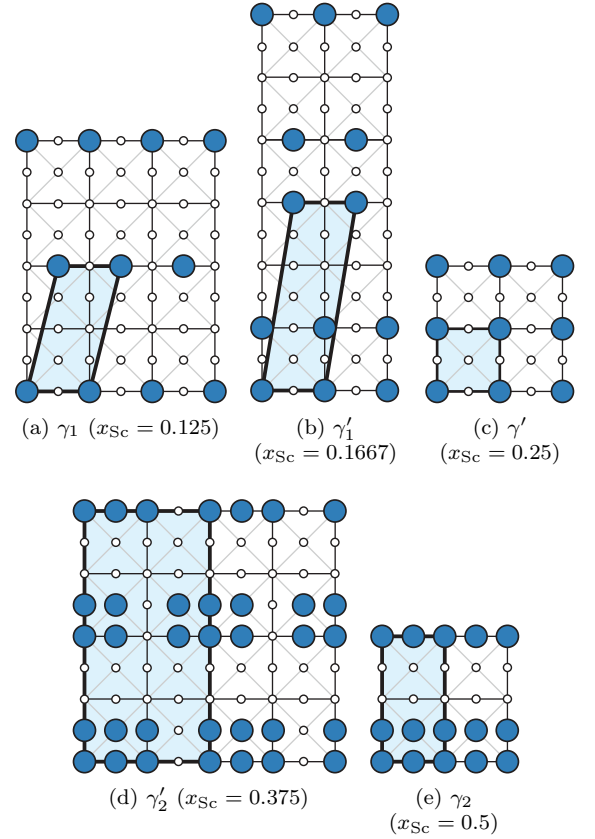(f) δ' $(x_{Sc} = 0.4)$

(g) β $(x_{Sc} = 0.5)$

FIG. 5. Schematic crystal structures of orderings on the metastable BCC convex hull. Scandium atoms are drawn in red and magnesium atoms are depicted by the smaller white circles. Crystal structures are viewed along [001]. Some orderings contain fully filled columns of scandium atoms, which are depicted as filled circles. Other orderings consisting of alternating scandium and magnesium atoms are shown as half filled circles, similar to the depiction of a partial occupancy on a sublattice. Since neighboring chains of Sc and Mg atoms can either be stacked "in-phase", where scandium atoms are all on the same layer and magnesium atoms are on adjacent layers or "out-of-phase", the filling of the circle is used to depict how neighboring chains are oriented relative to each other.

B. Global phase stability

The global phase stability across all orderings on the BCC, HCP and FCC crystal structures at 0K is shown

(a) γ_1 $(x_{Sc} = 0.125)$

(b) γ_1'
$(x_{Sc} = 0.1667)$

(c) γ'
$(x_{Sc} = 0.25)$

(d) γ_2' $(x_{Sc} = 0.375)$

(e) γ_2
$(x_{Sc} = 0.5)$

FIG. 6. Schematic crystal structures of orderings on the metastable FCC convex hull. Scandium atoms are drawn in blue and magnesium atoms are depicted by the smaller white circles. Crystal structures are viewed along [001]. Relative to this zone axis, the crystal structure can be viewed as a stacking of two centered square lattices that are shifted relative to each other. The atoms at the corners and center of a square belong to one layer, while the atoms at the edge centers are in the layer above.

in fig. 7. Pure magnesium and scandium are HCP at 0K. The HCP-based β_S''' family of orderings is found to be globally stable at compositions ranging between $x_{Sc} = 0.125$ to $x_{Sc} = 0.25$. Surprisingly the β_S' ordering with a composition of $x_{Sc} = 0.125$ is energetically degenerate with the FCC γ_1 ordering at the same composition. Up to a composition of 0.25, the FCC based orderings are within a few meV of the convex hull, but are higher in energy than the HCP orderings. For x_{Sc} ranging between 0.25 up to 0.5, FCC-based γ_2' and γ_2 orderings are stable. The HCP crystal structure is preferred again at higher values of x_{Sc} with the β_2 ordering forming at $x_{Sc} = \frac{2}{3}$.

The experimental phase diagrams show that BCC based orderings form in this binary alloy[3,8–12]. Our first-principles calculations suggest that BCC orderings are metastable at 0K. As is evident in fig. 2, BCC phases have energies above the the global convex hull at the extreme compositions, i.e. $x_{Sc} = 0$ and $x_{Sc} = 1$. However, BCC orderings around a composition of $x_{Sc} = 0.35$ show

rods from the γ_2 phase at regular intervals (in fig. 6d the interval is 3). Very short intervals, i.e. less than 3, are not found to be energetically favorable.
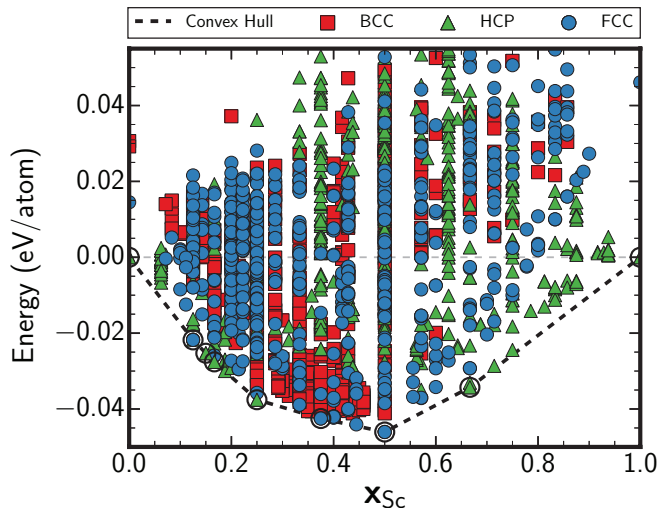
FIG. 7. DFT calculated formation energies of orderings on all three crystal structures: HCP (green triangles), BCC (red squares) and FCC (blue circles). Orderings on the global convex hull are circled.

a large drop in formation energies, bringing some within a few meV of the global convex hull. These low energy configurations on the BCC structure, shown in figs. 5d and 5f, can be viewed as Mg-Sc orderings on the Sc-rich sublattice of β (B2 or CsCl-type).

IV. FINITE TEMPERATURE PHASE STABILITY

Statistical mechanics methods based on the cluster expansion approach and Monte Carlo simulations were used to calculate finite temperature free energies and composition versus temperature phase diagrams. Three different configurational cluster expansions (eq. (2)), one for each crystal structure, were parametrized using the first-principles formation energies of Figures 1-3. The cluster expansions were used as input to grand canonical Monte Carlo simulations to generate finite temperature thermodynamic quantities for use in free energy integration schemes to predict finite temperature phase stability. Second order phase transitions were estimated by inspection of inflection points in temperature versus composition curves and corresponding peaks in heat capacities at constant chemical potential as calculated with grand canonical Monte Carlo simulations.

All three cluster expansions reproduce the formation energies of configurations to within a few meV/atom for the low energy orderings and have a root mean square error across all configurations of around 8 meV/atom (table I). Each cluster expansion is able to predict the strong DFT ground state orderings as residing on the convex hull of the parent crystal structure they describe. These are the orderings that are stable in a wide chemical potential window at zero Kelvin. Furthermore, the

cluster expansions do not predict any new ground states whose energies have not been calculated with DFT (See Appendix A for more details). Many of the more complex hierarchical ground state orderings, however, are not predicted as ground states by the parameterized cluster expansions. These hierarchical orderings are predicted by DFT to be weakly stsable ground states in that they barely break the convex hull and are therefore only stable in a very narrow chemical potential window. The cluster expansions predict their energies to be either degenerate with simpler ground state orderings (i.e. reside on a zero Kelvin common tangent) or to have formation energies that are only several meV/atom above the convex hull. The inability to predict the larger and more complex hierarchical phases as ground states can be attributed to the truncation of the cluster expansions beyond a finite interaction distance. Larger clusters are likely to stabilize the more complicated orderings. However, the weak stability of the higher order hierarchical phases at zero Kelvin suggests that they have relatively low order/disorder transition temperatures. In fact, the BCC cluster expansion is able to predict δ' (fig. 5e), one of the hierarchical orderings on BCC, as residing on the convex hull and Monte Carlo simulations predict that it disorders around 300K. Since the cluster expansions do not capture the subtle, very long-range, interactions responsible for the stability of the weak hierarchical phases, which is only of importance at low temperature, they are unable to accurately resolve the true equilibrium phase diagrams at low temperature where DFT predicts that the hierarchical ground state orderings coexist with the strong ground states. We, therefore only show calculated phase diagrams above 400K where only the strong ground state orderings that are accurately described with the cluster expansions remain stable.

Figure 8 shows the calculated metastable phase diagram for the HCP crystal structure. Our calculations predict the β'' and β_2 orderings to be stable until approximately 700K. Both ordered phases tolerate some degree of magnesium excess relative to their stoichiometric composition at elevated temperatures but only allow a negligible scandium excess. A disordered solid solution is predicted at high temperature and at both magnesium and scandium rich compositions. The ordered phases undergo first-order phase transitions to the solid solution at around 700K.

In contrast to the first-order phase transitions predicted for the HCP based orderings, BCC orderings are predicted to undergo a series of second order phase transitions as shown by the dashed lines in fig. 9. The metastable phase stability in this system has similarities with the well studied Fe-Al binary[36,37]. Three low temperature orderings are predicted in the BCC phase diagram: β_1 ($x_{Sc} = 0.25$), δ' ($x_{Sc} = 0.375$) and β ($x_{Sc} = 0.5$). The δ' ordering is predicted to be stable only up to about 300K. At higher temperatures, the ordered β_1 phase undergoes a second-order phase transition into β. This second order transition is possible due to
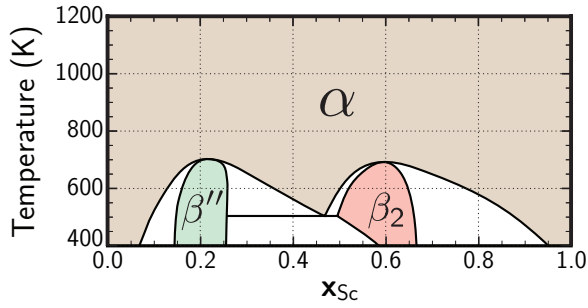
FIG. 8. Metastable phase diagram for HCP calculated using finite temperature free energies from Monte Carlo simulations applied to a configurational cluster expansion. Single phase fields are colored and labeled.
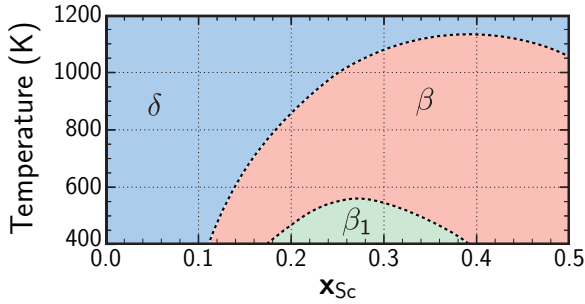

FIG. 9. Metastable phase diagram for BCC calculated using finite temperature free energies from Monte Carlo simulations applied to a configurational cluster expansion. Single phase fields are colored and labeled. Dashed lines represent second-order phase transitions.

the group/subgroup relationship between the β and β_1 orderings. At temperatures above 500K the β phase becomes stable over a wide concentration interval, similar to what is observed experimentally. At high enough temperatures, the β phase eventually disorders into a solid-solution.

The metastable FCC phase diagram (fig. 10) shows a number of invariant peritectoid reactions. Most orderings, with the exception of γ_2, do not tolerate much off-stoichiometry and undergo first-order phase transitions to a high temperature FCC solid solution. The γ_2 phase is predicted to have a large magnesium solubility at higher temperatures and undergoes a second-order phase transition to the disordered solid solution. Similar to the BCC and HCP metastable phase diagrams, the low-temperature ordered phases are stable up to about 600K.

V. DISCUSSION

First-principles calculations reveal the stability of complex hierarchically ordered ground states across the HCP, BCC and FCC crystal structures at 0K. This is similar to other Mg-RE alloys that exhibit long period
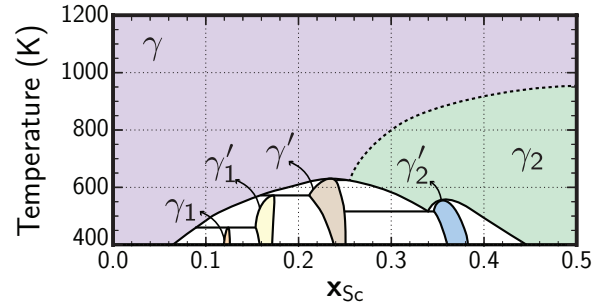

FIG. 10. Metastable phase diagram for FCC calculated using finite temperature free energies from Monte Carlo simulations applied to a configurational cluster expansion. Single phase fields are colored and labeled. Dashed lines represent second-order phase transitions.

orderings[4,5,38]. The calculated metastable phase diagrams for HCP, BCC and FCC Mg-Sc alloys of figs. 8 to 10 display a rich variety of order/disorder phase transitions. In all three metastable phase diagrams, the Mg rich orderings disorder around 600K to form either a disordered solid solution or a highly off-stoichiometric ordered phase. The metastable BCC phase diagram is especially remarkable with its very wide stability range of the B2 ordering, which is predicted to accommodate an excess Mg concentration of more than 0.3 relative to the ideal B2 stoichiometric composition of $x_{Sc} = 0.5$. These predictions show that configurational entropy plays a crucial role in determining the thermodynamic properties of Mg-Sc alloys at intermediate to high temperatures.

Figure 11 shows calculated free energies that rigorously account for configurational degrees of freedom for HCP, BCC and FCC at 772 K. The free energy diagram clearly reveals a very high degree of degeneracy among the three phases in a Sc composition interval between $x_{Sc} = 0.2$ and 0.5. This also happens to be the composition interval in which shape memory phenomena were recently observed by Ogawa et al.[3]. The degeneracy at high temperature is already present at zero Kelvin where the formation energies of ordered ground states on HCP, BCC and FCC are all within a few meV from each other in the same composition interval. The high degree of degeneracy among HCP, FCC and BCC likely plays an important role in determining the mechanisms with which this alloy system manifests shape memory behavior.

The equilibrium phase diagram calculated by applying the common tangent construction to the configurational free energies of all three crystal structures is shown in fig. 12. The phase diagram predicts the formation of HCP and FCC based orderings at intermediate to low temperatures and an HCP solid solution at high temperature. The phase diagram does not agree with experimental studies[3,8–12] as it does not predict BCC to be stable. Experiments have shown the formation of a high-temperature BCC phase at intermediate scandium compositions (around $x_{Sc} = 0.3 - 0.5$).

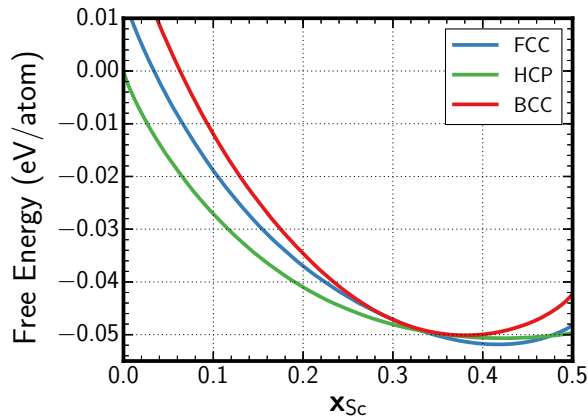We can identify several reasons as to why the pre-

FIG. 11. Free energies of the BCC, HCP and FCC crystal structures calculated using the cluster expansion, Monte Carlo simulations and free energy integration at 772K
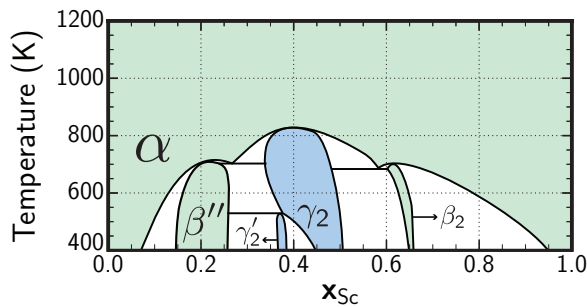

FIG. 12. The global phase diagram, accounting for the finite temperature phase stability of all three crystal structures. Single phase fields are colored and labeled, with HCP based phases shown in green and FCC based phase fields shown in blue.

dicted equilibrium phase diagram is inconsistent with high temperature experiments. First, the degeneracy among the three phases between $x_{\text{Sc}} = 0.2$ and 0.5 (fig. 11) leads to free energy differences that are of the same order as numerical errors associated with the DFT calculations and cluster expansion parameterization of DFT formation energies. More importantly, the free energies of fig. 11 neglect contributions from vibrational excitations[32,39–41] and entropy due to point defect formation at high temperatures[42,43]. It is empirically known that more open crystal structures such as BCC tend to have a higher vibrational entropy than the more tightly bound close packed crystal structures such as HCP and FCC[39,40]. Therefore, we expect that the inclusion of vibrational excitations will decrease the free energy of BCC more than those of HCP and FCC with increasing temperature.

While accounting for vibrational excitations is computationally very demanding, especially in phases also exhibiting configurational disorder, we can estimate their importance by empirically shifting the free energy of the

BCC phase relative to those of HCP and FCC to match high temperature features of the experimental phase diagram. The simplest approximation is to assume that the vibrational contributions to the free energies of the close packed FCC and HCP phases are similar, but that those to the BCC free energy are different. To represent this difference, we introduce an excess free energy for the BCC phase relative to both HCP and FCC, $\Delta G_{\text{xs}}^{\text{BCC}}$, that can be added to the BCC configurational free energy. The excess free energy can be parameterized with a simple temperature (T) and composition (x_{Sc}) dependence:

$$\Delta G_{\text{xs}}^{\text{BCC}} = (a_0 + a_1 x_{\text{Sc}})T + (b_0 + b_1 x_{\text{Sc}})T \ln T \quad (3)$$

where $\{a_0, a_1, b_0, b_1\}$ are fitting coefficients. At constant temperature, this excess free energy provides a rigid shift as well as a linear offset to the BCC free energy relative to that of FCC and HCP. Neither of these modifications will change the metastable phase diagram shown in fig. 9. To fit the coefficients in eq. (3), we used the two-phase equilibrium data from the diffusion couple study of Ogawa *et al.* Diffusion couples provide accurate estimates of the phase boundaries between different phase fields.

Shifting the BCC free energies by augmenting the configurational free energies calculated from first-principles with experimental data leads to a qualitatively different phase diagram as shown in fig. 13. The two-phase field between α (disordered HCP) and β (disordered CsCl-type) is reproduced in this phase diagram as reported in previous experimental studies. Although experiments suggest the formation of a completely disordered BCC solid solution, we predict a Mg excess B2 phase characterized by Mg-Sc disorder over the Sc sublattice to be stable at the experimental temperatures. Many other two-phase regions appear in fig. 13 due to the lowered free energies of the BCC phase, including BCC-FCC two-phase fields. Low temperature phase stability remains unaffected since the excess free energy, as parameterized with Eq. 3, tends to zero as T approaches 0K.

The magnitude of free energy shifts required to replicate the experimental two-phase field are very small. In the composition region we are fitting to, free energy shifts are of the order of 10 meV/atom at a temperature of 953K and are sufficient to reproduce the experimental data at high temperature. The calculated phase diagram is, therefore, very sensitive to small relative shifts of the individual free energies. While we have argued that a sizable fraction of the shift that is required to reproduce the high temperature phase diagram is likely due to differences in vibrational entropy between BCC and the close-packed FCC and HCP phases, the empirical shifts of eq. (3) undoubtedly also account for errors arising from approximations to DFT and cluster expansion fitting errors. The exact source is difficult to single out due to the very small magnitude of the excess free energy.

Though the exact phase stability might be difficult to resolve in this system, the small differences in free energies at elevated temperatures suggests the importance of the FCC phase in the Mg-Sc system either as an easily
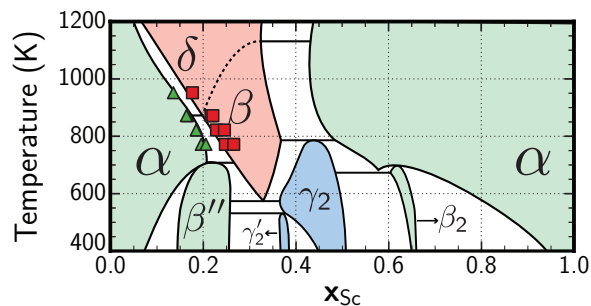
FIG. 13. Re-calculated phase diagram, based on empirical shifts to the configurational free energies of BCC based phases. Shifts are parameterized using the data from diffusion couples as reported by Ogawa *et al.*[11]. Single phase fields are colored and labeled, with HCP based phases shown in green, FCC based phase fields shown in blue and BCC phase fields shown in red. The experimental phase boundaries from the study by Ogawa *et al.*[11] are also shown, with the β phase field as red squares and the α phase fields as green triangles. The BCC free energy was shifted by: $(0.1 - 0.13x_{Sc})T + (-0.0169 + 0.0229x_{Sc})T \ln T$ meV/atom

accessible metastable phase or as a thermodynamically stable phase at low temperatures. The formation of a FCC based phase has never been reported in this system. The formation energies of all three crystal structures (BCC, FCC and HCP) are very close at lower temperature. However, our predictions suggest that FCC is consistently lower in energy than BCC for low scandium compositions. As a result, any quenching heat treatments at compositions ranging between $x_{Sc} = 0.2 - 0.5$ may promote martensitic phase transformations to both HCP and FCC. The FCC based martensites would be expected to form through a Bain transformation from the BCC solid solution. Some degree of tetragonality may be expected for these martensites due to both the symmetry of the ordering and any remnant local stresses/strains. These FCC based martensites, if formed, may be related to the shape memory phenomena that has been reported in this alloy system[3].

In addition to exhibiting a high degree of degeneracy between HCP, BCC and FCC, the Mg-Sc binary also favors an intriguing array of complex ordered phases at low temperature. Remarkably, the ground state orderings on all three crystal structures share many common features. All the low-energy configurations (either metastable or stable) consist of scandium rods arranged as clusters or layers that arrange two-dimensionally. Many ground state orderings consist of several layers of pure magnesium locally adopting an FCC or BCC crystal structure, even though pure Mg is either highly metastable or unstable in FCC and BCC. Also striking is the large number of hierarchical phases that are stable or metastable in all three crystal structures. The two dimensional nature of the many ground state orderings make them readily discernible using HAADF-STEM (high angle annular dark field-scanning transmission elec-

tron microscopy)[2,4,5] when viewed along the appropriate zone axis.

VI. CONCLUSION

We have performed a first-principles statistical mechanics study of phase stability in the Mg-Sc binary. Our calculations predict that ordered and disordered phases on HCP, BCC and FCC have energies and free energies that are very close to each other between $x_{Sc} = 0.2 - 0.5$, corresponding to compositions where shape memory effects have recently been observed[3]. The predicted stability of FCC based orderings is especially surprising since they are not observed in high-temperature experiments. Ground-state orderings on all three crystal structures are found to contain rods of scandium atoms arranged in layers, with adjacent layers being separated from each other by blocks of magnesium. Monte Carlo simulations applied to first-principles cluster expansions for HCP, BCC and FCC predict a rich variety of order/disorder transitions. The calculated metastable BCC phase diagram is especially interesting as it contains a B2 phase field that exhibits a very wide solubility range, with excess magnesium accommodated on the scandium sublattice. This prediction is consistent with limited high temperature experimental information. Empirical shifts to the free energy of BCC using inputs from past diffusion couple experiments[11] showed that small differences in the vibrational entropy could be responsible for the experimentally observed BCC phases at high temperatures. The predicted degeneracy of FCC based phases with HCP may be a key to unraveling mechanisms and crystallographic pathways of martensitic transformations responsible for the observed shape memory alloys in quenched BCC Mg-Sc alloys.

Appendix A: Cluster Expansion Fits

Formation energies predicted from three different cluster expansions across the HCP, BCC and FCC crystal structures are shown in figs. 14a to 14c. The cluster expansions are trained to reproduce the important features of the formation energies calculated from DFT. The strong ground states (orderings that are stable in a wide chemical potential interval) are reproduced very accurately by the cluster expansions, with the more complicated orderings predicted to be either degenerate or nearly degenerate in energy.

The HCP cluster expansion (fig. 14a) predicts the important orderings (β'' and β_2) to be thermodynamically stable, while the hierarchical β''' orderings are very close in energy to the predicted convex hull but not on the hull. The BCC cluster expansion (fig. 14b) is trained to reproduce the ground states with compositions between $x_{Sc} = 0.25 - 0.5$. This corresponds to the composition region where BCC orderings are found to be energetically competitive relative to the global ground states. The FCC based cluster expansion is trained to predict orderings with compositions less than $x_{Sc} = 0.5$. The γ'_1 ordering predicted by the cluster expansion is energetically degenerate based on the DFT calculations. The DFT calculations predict the γ_1 ordering on FCC to be energetically degenerate with the β'_S ordering on HCP, both orderings have a composition of $x_{Sc} = 0.125$. This degeneracy is not reproduced by the two cluster expansions presented in this study. The orderings are within 4 meV/atom of each other based on the predictions, which is within the numerical accuracy of our cluster expansions. The cluster expansions are however in qualitative agreement with the DFT calculations.

The global phase stability predicted by the cluster expansions and the DFT calculations are shown in fig. 15. The formation energies predicted are very close to the calculated values. In the context of global phase stability, the stronger ground states are reproduced well, i.e. β'', β_2 and γ_2. The γ'_2 ordering is also predicted to be globally stable similar to the calculated DFT formation energies. The cluster expansions however differ slightly from the DFT calculations at scandium poor compositions with the β'''_S and γ_1 orderings not being reproduced. However, these are more complicated hierarchical orderings and are expected to disorder at relatively low temperatures. Further, reproducing such orderings with truncated cluster expansions typically requires very large cluster sizes.
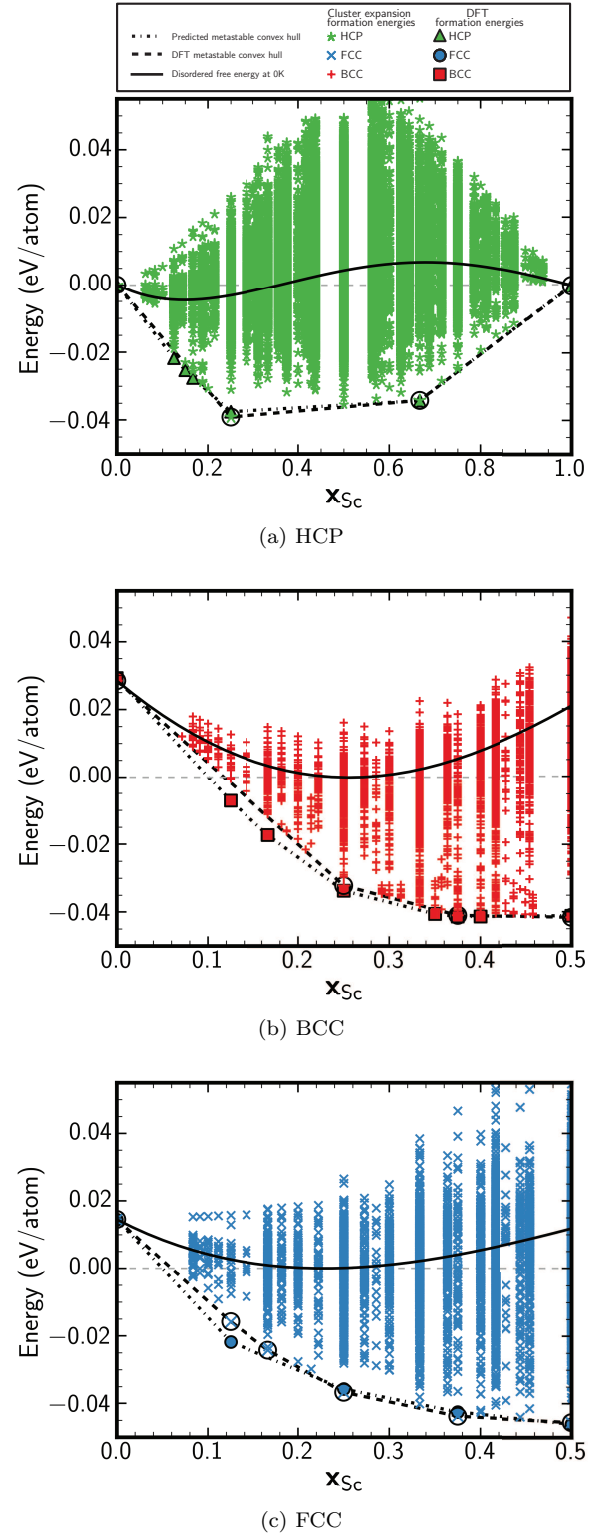

(a) HCP

(b) BCC

(c) FCC

FIG. 14. Predicted energies from the three different cluster expansion fits. Each figure shows the metastable convex hull predicted by the cluster expansion fit, as well as the metastable hull from the DFT calculations. The disordered free energy at 0K is also shown as a solid line. Configurations that are on the cluster expansion convex hull are circled.
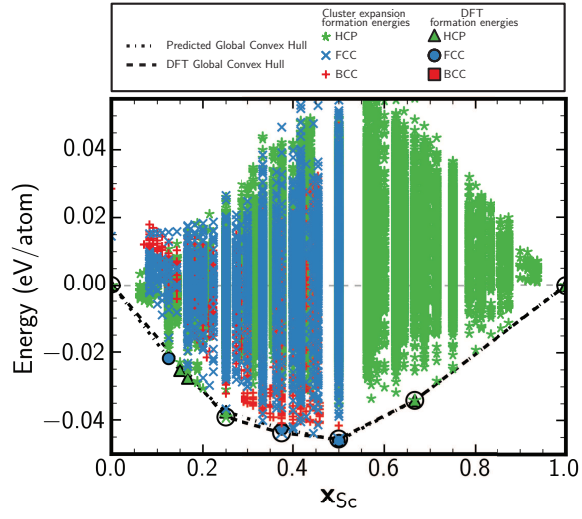
FIG. 15. Formation energies across orderings on HCP, BCC and FCC as predicted from three cluster expansions. The configurations on global convex hull are circled, and correspond to β'', γ_1', γ_1, and β_2. The predicted DFT convex hull is also shown with solid symbols.

[*] avdv@engineering.ucsb.edu
[1] T. M. Pollock, Science **328**, 986 (2010).
[2] J.-F. Nie, Metallurgical and Materials Transactions A **43**, 3891 (2012).
[3] Y. Ogawa, D. Ando, Y. Sutou, and J. Koike, Science **3**, 30 (2016).
[4] A. R. Natarajan, E. L. S. Solomon, B. Puchala, E. A. Marquis, and A. Van der Ven, Acta Materialia **108**, 1 (2016).
[5] A. R. Natarajan and A. Van der Ven, Acta Materialia (2016), 10.1016/j.actamat.2016.10.057.
[6] A. Issa, J. Saal, and C. Wolverton, Acta Materialia **65**, 240 (2014).
[7] A. Issa, J. Saal, and C. Wolverton, Acta Materialia **83**, 75 (2015).
[8] B. J. Beaudry and A. H. Daane, Journal of the Less Common Metals **18**, 305 (1969).
[9] J. Grobner, R. Schmid-Fetzer, A. Pisch, G. Cacciamani, P. Riani, N. Parodi, G. Borzone, A. Saccone, and R. Ferro, Zeitschrift fur Metallkunde **90**, 872 (1990).
[10] A. Pisch, R. Schmid-Fetzer, G. Cacciamani, P. Riani, A. Saccone, and R. Ferro, Zeitschrift fur Metallkunde **89**, 474 (1998).
[11] Y. Ogawa, D. Ando, Y. Sutou, K. Yoshimi, and J. Koike, Materials Science and Engineering: A **670**, 335 (2016).
[12] Y. Ogawa, D. Ando, Y. Sutou, and J. Koike, Magnesium Technology 2016 , 147 (2016).
[13] R. H. Taylor, S. Curtarolo, and G. L. W. Hart, Physical Review B **84**, 084101 (2011).
[14] P. Lazar, M. Jahnátek, J. Hafner, N. Nagasako, R. Asahi, C. Blaas-Schenner, M. Stöhr, and R. Podloucky, Physical Review B - Condensed Matter and Materials Physics **84**, 1 (2011).
[15] T. Chakraborty, J. Rogal, and R. Drautz, Journal of Physics: Condensed Matter **27**, 115401 (2015).
[16] T. Chakraborty, J. Rogal, and R. Drautz, Physical Review B **94** (2016), 10.1103/PhysRevB.94.224104.
[17] K. Guda Vishnu and A. Strachan, Acta Materialia **58**, 745 (2010).
[18] D. Holec, M. Friák, A. Dlouhý, and J. Neugebauer, Physical Review B **84** (2011), 10.1103/PhysRevB.84.224119.
[19] N. A. Zarkevich and D. D. Johnson, Physical Review Letters **113** (2014), 10.1103/PhysRevLett.113.265701.
[20] N. A. Zarkevich and D. D. Johnson, Physical Review B **90** (2014), 10.1103/PhysRevB.90.060102.
[21] W.-S. Ko, B. Grabowski, and J. Neugebauer, Physical Review B **92** (2015), 10.1103/PhysRevB.92.134107.
[22] X. Huang, G. J. Ackland, and K. M. Rabe, Nature materials **2**, 307 (2003).
[23] J. P. Perdew, K. Burke, and M. Ernzerhof, Physical Review Letters **77**, 3865 (1996).
[24] G. Kresse and J. Hafner, Physical Review B **47**, 558 (1993).
[25] G. Kresse and J. Furthmüller, Physical Review B **54**, 11169 (1996).
[26] G. Kresse and J. Furthmüller, Computational Materials Science **6**, 15 (1996).
[27] G. Kresse and J. Hafner, Physical Review B **49**, 14251 (1994).
[28] J. Sanchez, F. Ducastelle, and D. Gratias, Physica A: Statistical Mechanics and its Applications **128**, 334 (1984).
[29] D. de Fontaine, Solid state physics **47**, 33 (1994).
[30] D. de Fontaine, Solid State Physics **47**, 73 (1979).
[31] CASM Developers, "CASM: A Clusters Approach to Statistical Mechanics," (2016).
[32] J. C. Thomas and A. Van der Ven, Physical Review B **88**, 214111 (2013).
[33] B. Puchala and A. Van Der Ven, Physical Review B - Condensed Matter and Materials Physics **88**, 1 (2013).
[34] A. Van der Ven, J. C. Thomas, Q. Xu, and J. Bhattacharya, Mathematics and Computers in Simulation **80**, 1393 (2010).
[35] G. L. W. Hart, V. Blum, M. J. Walorski, and A. Zunger, Nature materials **4**, 391 (2005).
[36] S. Allen and J. Cahn, Acta Metallurgica **27**, 1085 (1979).
[37] B. B. Lindahl, B. P. Burton, and M. Selleby, Calphad **51**, 211 (2015).
[38] J.-K. Kim, W.-S. Ko, S. Sandlbes, M. Heidelmann, B. Grabowski, and D. Raabe, Acta Materialia **112**, 171 (2016).
[39] A. Van De Walle and G. Ceder, Reviews of Modern Physics **74**, 11 (2002).
[40] B. Fultz, Progress in Materials Science **55**, 247 (2010).
[41] A. Glensk, B. Grabowski, T. Hickel, and J. Neugebauer, Phys. Rev. Lett. **114**, 195901 (2015).
[42] A. A. Belak and A. Van der Ven, Phys. Rev. B **91**, 224109 (2015).
[43] A. Glensk, B. Grabowski, T. Hickel, and J. Neugebauer, Phys. Rev. X **4**, 011018 (2014).
[44] B. Puchala, G. Tarcea, E. A. Marquis, M. Hedstrom, H. V. Jagadish, and J. E. Allison, JOM **68**, 2035 (2016).
[45] www.materialscommons.org.
[46] J. D. Hunter, Computing In Science & Engineering **9**, 90 (2007).